doi:10.1038/nature19065

A progressively wetter climate in southern East Africa over the past 1.3 million years

T. C. Johnson[1,2], J. P. Werne[3], E. T. Brown[1], A. Abbott[4], M. Berke[5], B. A. Steinman[1], J. Halbur[1], S. Contreras[6], S. Grosshuesch[1], A. Deino[7], R. P. Lyons[8]†, C. A. Scholz[8], S. Schouten[9,10] & J. S. Sinninghe Damsté[9,10]

African climate is generally considered to have evolved towards progressively drier conditions over the past few million years, with increased variability as glacial–interglacial change intensified worldwide[1–3]. Palaeoclimate records derived mainly from northern Africa exhibit a 100,000-year (eccentricity) cycle overprinted on a pronounced 20,000-year (precession) beat, driven by orbital forcing of summer insolation, global ice volume and long-lived atmospheric greenhouse gases[4]. Here we present a 1.3-million-year-long climate history from the Lake Malawi basin (10°–14° S in eastern Africa), which displays strong 100,000-year (eccentricity) cycles of temperature and rainfall following the Mid-Pleistocene Transition around 900,000 years ago. Interglacial periods were relatively warm and moist, while ice ages were cool and dry. The Malawi record shows limited evidence for precessional variability, which we attribute to the opposing effects of austral summer insolation and the temporal/spatial pattern of sea surface temperature in the Indian Ocean. The temperature history of the Malawi basin, at least for the past 500,000 years, strongly resembles past changes in atmospheric carbon dioxide and terrigenous dust flux in the tropical Pacific Ocean, but not in global ice volume. Climate in this sector of eastern Africa (unlike northern Africa) evolved from a predominantly arid environment with high-frequency variability to generally wetter conditions with more prolonged wet and dry intervals.

Rainfall is the key metric for eastern African climate; annual temperature variations are limited, while moisture availability is far less predictable and profoundly affects distributions of vegetation and habitability across the landscape. Proxy records of northern and eastern African palaeoclimate reveal a trend towards drier conditions over the past few million years, overprinted by Milankovitch-scale cycles tied to Earth's orbit about the Sun[1,2,5]. However, it is unclear whether this trend holds for all of Africa. Our objectives were to determine how temperature and rainfall in the Malawi basin responded to orbital forcing of summer insolation, and whether they tracked global records of climate change, such as ice volume[6] and atmospheric carbon dioxide[7],

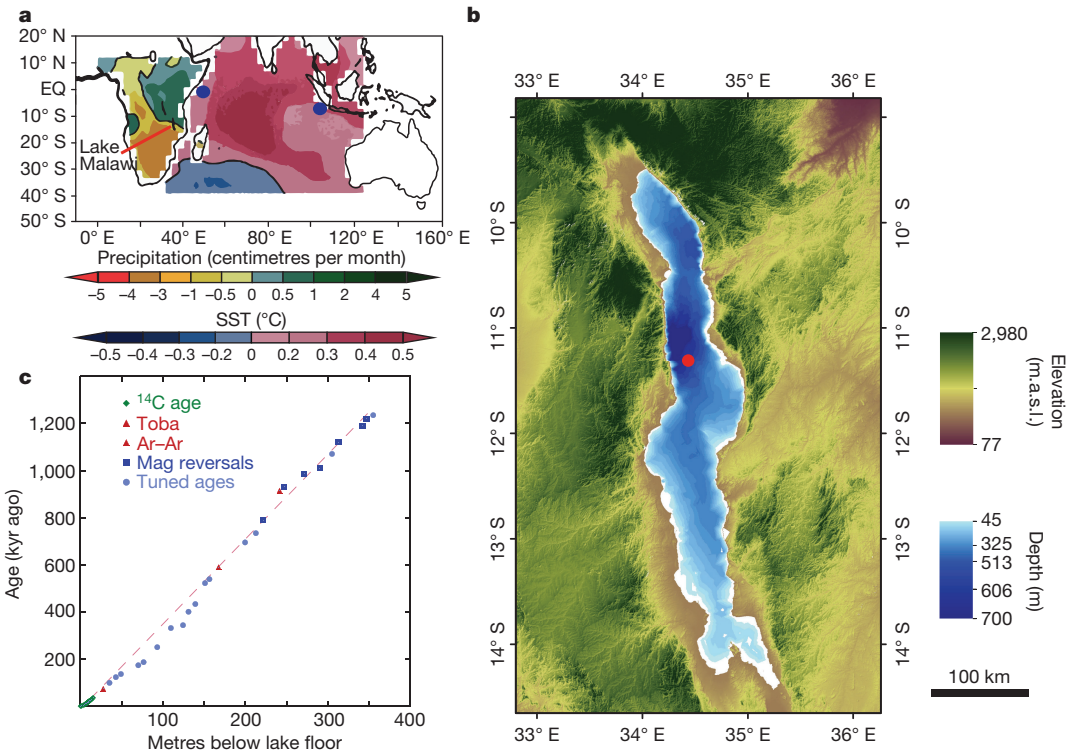

Figure 1 | The location and bathymetry of Lake Malawi, African rainfall response to the Indian Ocean dipole, and the drill site age model. **a**, Dominant patterns of precipitation variability over Africa and SST variability over the Indian Ocean for November–December–January of 1970–1992 (modified from ref. 24). The two blue dots depict the locations of two cores used to derive the history of west-minus-east SST gradient in Fig. 3 (see Methods). **b**, Bathymetric map of Lake Malawi, with location of drill site MAL05-1 (red dot), and digital elevation (metres above sea level, m.a.s.l.) map of the catchment. **c**, The age model for drill site MAL05-1.

[1]Large Lakes Observatory and Department of Earth and Environmental Sciences, University of Minnesota Duluth, Duluth, Minnesota 55812, USA. [2]Department of Geosciences, University of Massachusetts Amherst, Amherst, Massachusetts 01003, USA. [3]Department of Geology and Planetary Science, University of Pittsburgh, Pittsburgh, Pennsylvania 15260, USA. [4]Department of Earth and Planetary Sciences, Faculty of Science and Engineering, Macquarie University, Sydney, New South Wales 2109, Australia. [5]Department of Civil & Environmental Engineering & Earth Sciences, University of Notre Dame, 257 Fitzpatrick Hall, Notre Dame, Indiana 46556, USA. [6]Departamento de Química Ambiental and Centro de Investigación en Biodiversidad y Ambientes Sustentables (CIBAS), Universidad Católica de la Santísima Concepción, Casilla 297, Concepción, Chile. [7]Berkeley Geochronology Center, 2455 Ridge Road, Berkeley, California 94709, USA. [8]Earth Sciences Department, Syracuse University, 011a Heroy Geology Laboratory, Syracuse, New York 13244, USA. [9]NIOZ Netherlands Institute for Sea Research, Department of Marine Microbiology and Biogeochemistry, and Utrecht University, PO Box 59, 1790 AB Den Burg, The Netherlands. [10]Faculty of Geosciences, Department of Earth Sciences, Utrecht University, PO Box 80.021, 3508 TA Utrecht, The Netherlands. †Present address: Chevron Corporation, 1400 Smith Street, Houston, Texas 77002, USA.

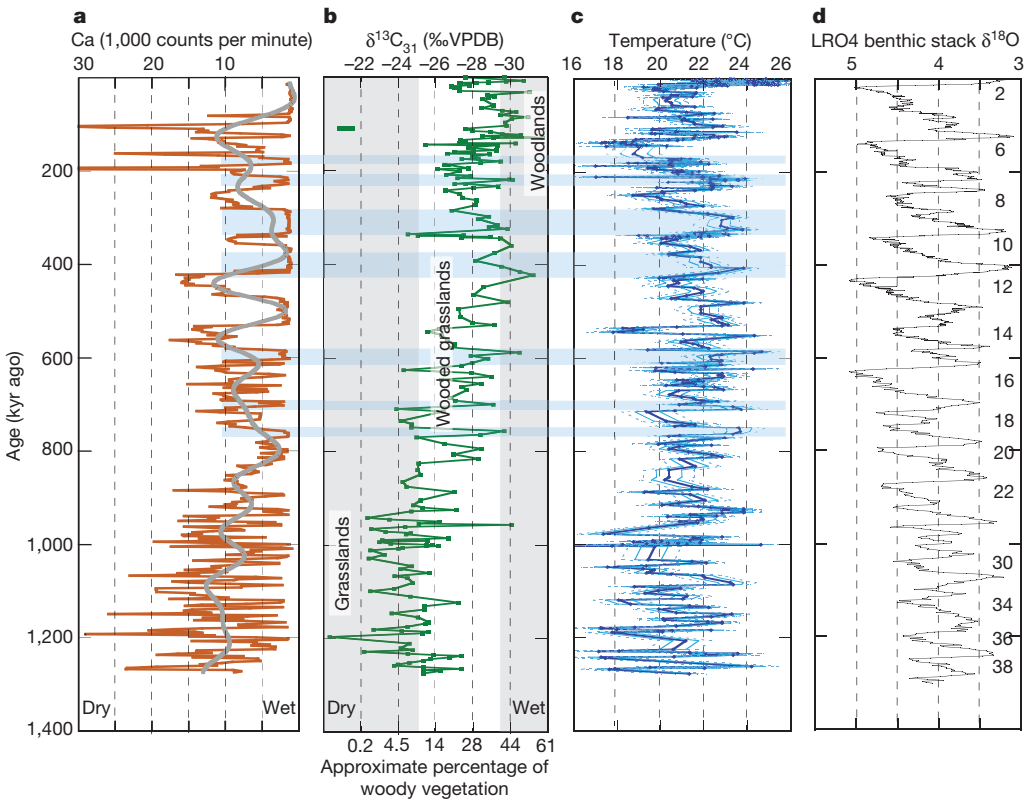

Figure 2 | Vegetation (hydroclimate) and temperature history of the Lake Malawi basin. a, Profile of calcium abundance ($n = 22{,}010$), determined by X-ray fluorescence analysis at about 2-cm intervals, followed by a 20-point running mean. **b**, Profile of $\delta^{13}C_{31}$ ($n = 207$); each sample was run at least in duplicate and co-injected with squalane as an internal standard to monitor reproducibility of measurements. **c**, Profile of corrected temperature ($n = 406$); roughly 10% of the samples were run in duplicate, and displayed average differences in TEX_{86} of 0.0076, corresponding to a 2σ temperature value of 0.8 °C. **d**, Profile of LR04 with marine isotope stage (MIS) numbers for glacial periods identified[6] ($n = 950$). The heavy grey line in **a** represents a 100-kyr low-pass filter through the calcium data, which highlights the progressively wetter mean climate of the Malawi basin over the past 1.3 million years, as do the $\delta^{13}C_{31}$ data. The green bar in the upper left corner of **b** indicates $\pm 1\sigma$ analytical uncertainty in $\delta^{13}C_{31}$. 1σ and 2σ uncertainties in temperature due to analytical and lapse rate corrections (Methods) are indicated by the light blue solid and dashed lines, respectively, in **c**. Blue-shaded bars highlight some wet intervals, illustrating their correlation with warm temperatures during interglacial periods. Percentage woody vegetation is estimated from the $\delta^{13}C_{31}$ correlation of ref. 16.

as well as the trends of increased aridity and variability observed farther north in Africa.

Although Lake Malawi (Fig. 1a) is an open basin today, its surface has dropped well below the elevation of its outlet on numerous occasions, creating closed-basin conditions with attendant shoreline migration and elevated water salinity[8,9]. We analysed sediment samples recovered by the Lake Malawi Drilling Project to produce records of temperature (TEX_{86}) and aridity (calcium (Ca) content and leaf wax $\delta^{13}C_{31}$, where C_{31} indicates an *n*-alkane containing 31 carbon atoms) extending back to approximately 1.3 million years before present (Methods). Our age model for the sediment sequence is based on 15 radiocarbon dates, 3 dated tephra layers, and 6 palaeomagnetic reversals, supplemented by alignment of the TEX_{86} temperature record with the LR04 (the stacked record[6] of marine benthic foraminifera $\delta^{18}O$) to assign ages between 75 and 590 thousand years (kyr) ago (Fig. 1c) (Methods).

A cyclic structure is apparent in the TEX_{86} temperature record after 600 kyr ago (Fig. 2, Extended Data Fig. 1). This is overprinted by considerable variability throughout the entire sediment sequence; we attribute this variability to the ill-defined ecology of freshwater *Thaumarchaeota*, which produce the TEX_{86} signal (such as the preferred water depth for *Thaumarchaeota*, dominant species in the archaeal community, seasonal variability)[10,11], and to inter-seasonal and inter-annual lake circulation dynamics. The temperature varies with an amplitude of about 4 °C, between approximately 19 °C and 23 °C, displaying progressively larger-amplitude glacial–interglacial variations from marine isotope stage (MIS) 13 (about 500 kyr ago) to MIS 5 (about 125 kyr ago), after a remarkably cool MIS 14 (about 540 kyr ago) (Fig. 2c).

The degree of glacial cooling in the Malawi basin over the past 600 kyr does not match the amplitude of change in global ice volume as represented by the LR04 record (Fig. 2d). For example, Malawi basin glacial cooling was only about 2 °C during MIS 12, when continental ice sheets were particularly extensive, but was 4 °C during MIS 14, when global ice volume was relatively limited (Fig. 2c, d). However, the Malawi temperature record more closely matches the atmospheric carbon dioxide record for the past 600 kyr in the EPICA ice core[7] (Fig. 3a), and even more closely aligns ($R^2 = 0.363$ and 0.658, $P < 0.05$, on raw and 100-kyr low-pass-filtered data, respectively) with a 500-kyr record of terrigenous dust flux to the central equatorial Pacific[12] (Fig. 3b). These relationships reflect carbon dioxide's key role in regulating tropical eastern African temperatures on a glacial–interglacial timescale, and suggest that atmospheric dust may also have contributed to temperature regulation on these timescales, despite its modest radiative impact, estimated at an order of magnitude lower than that of greenhouse gases[13].

Calcium concentrations undergo a dramatic change from high-amplitude variability between calcareous and non-calcareous sediment (reflecting relatively arid and moist conditions, respectively) before 900 kyr ago to more prolonged periods of non-calcareous sediment and mainly lower-amplitude variations in the calcium values thereafter (Fig. 2a). Arid intervals were also longer after 900 kyr ago, including the most extreme 'mega-drought' of the past million years[9,14] which, if our tuned age model is correct, had its onset during MIS 6. Intriguingly, dry conditions when the lake surface was tens to hundreds of metres below outlet elevation (lowstand conditions) persisted intermittently well into

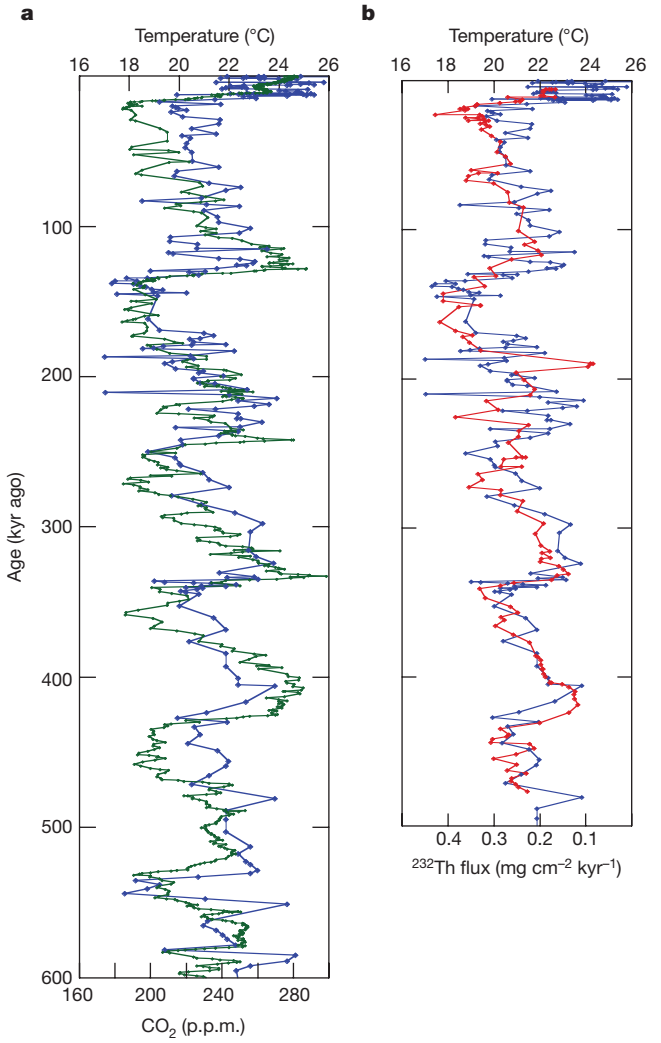

Figure 3 | Correlation of the Malawi temperature record with atmospheric carbon dioxide and dust. Temperature record for the Malawi basin (blue data points), plotted with atmospheric carbon dioxide (green data points)[7] (in **a**) and the dust flux to the central equatorial Pacific Ocean as represented by the depositional flux of ^{232}Th (red data points)[12] (in **b**).

MIS 5, when a final recovery to hydrologically overfilled conditions developed (Fig. 2a).

$\delta^{13}C_{31}$ displays variability within a range of about 4‰ throughout the record, superimposed on a trend towards more negative mean values from around −24.5‰ in the earlier part of the record to around −29‰ in the last 100,000 years. We attribute this trend to a gradual shift to wetter conditions, and not to a change in catchment (other than its expansion when lake level dropped). From the perspective of basin evolution, we observe no evidence for major changes in catchment geometry (such as drainage capture), or large alterations of topographic gradients or the deformational regime over the interval of the drill core. Earlier in the Malawi rift valley's history, major shifts in catchment geometry and basin physiography would have occurred, owing to continental extension. On the basis of the extensive seismic reflection data set available from the basin[15], such changes were unlikely in the most recent 15%–20% or so of the basin's history represented in our drill core.

$\delta^{13}C$ of vegetation can vary considerably, from about −24‰ to −35‰ for C_3 and from −11‰ to −14‰ for C_4 plants[16]. Nevertheless, an empirical relationship has been established between $\delta^{13}C$ of soil organic matter and fractional cover of woody vegetation ($r^2 = 0.77$) in eastern Africa[17]. This has been extended to $\delta^{13}C$ of C_{31} *n*-alkanes preserved in lake sediment[16]. We use this relationship to estimate the vegetation in the Malawi catchment at the time of biomarker deposition. Our measured values of $\delta^{13}C_{31}$ reflect substantial variations in the grassland cover, with less than 10% woody cover before 900 kyr ago, wooded grasslands consisting of 10%–40% woody plant cover and well developed ground cover of grasses and herbs from 900 kyr ago to the present, and occasional establishment of true woodlands, consisting of >40% woody plant cover in open or closed stands of trees, shrubs or thickets in the past 100 kyr (Fig. 2b).

After 900 kyr ago the calcium record displays intervals of carbonate-free sediment accumulation that lasted several tens of thousands of years, signifying open lake conditions during humid periods. These alternated with dry intervals, marked by carbonate accumulation, of comparable duration. The lake highstands correlate with periods of more negative $\delta^{13}C_{31}$ and relatively warm temperatures (Fig. 2). Thus the Malawi basin experienced warm, wet interglacials and cooler (by about 2–4 °C), dry glacial periods, with a roughly 100-kyr periodicity, if our assumed age model is correct, over the past 900 kyr (Extended Data Fig. 2). It is noteworthy that during the megadrought initiated in MIS 6, when Lake Malawi was reduced to a saline lake <100 m deep[9,14,18], the amplitude of the $\delta^{13}C_{31}$ shift was relatively small, about 5‰ (Fig. 2b). However, the relationship between $\delta^{13}C_{31}$ and landscape vegetation is nonlinear, so the relatively small 5‰ shift in $\delta^{13}C_{31}$ represents a fourfold decrease in woody vegetation from ~40% to ~10% of the land cover.

Holocene climate shifts linked to precessional forcing are reported throughout northern Africa and much of tropical eastern Africa (including the so-called "African Humid Period"[19]), but the anti-phased response in the Southern Hemisphere (that is, an early Holocene arid period) appears to have been subdued and intermittent (for example, an early Holocene drop of about 120 m in the level of Lake Malawi[20] interspersed with highstands[21]; brief, early Holocene highstands of Lake Makgadikgadi at about 20° S (ref. 22) and Lake Chilwa at about 15° S (ref. 23). The apparent lack of an approximately 20-kyr cycle in the hydroclimate of the Lake Malawi basin over the past 900 kyr (Extended Data Fig. 2) is consistent with this more recent history.

We attribute the limited precessional signal in the Malawi record to the opposing effects of orbital influence on summer insolation and the Indian Ocean Dipole (IOD) pattern of sea surface temperature (SST) variability. At present, rainfall is enhanced in tropical eastern Africa but diminished in southern Africa during positive IOD phases (warm western equatorial Indian Ocean relative to the eastern Indian Ocean), and vice versa[24]. The IOD shows strong precessional variability, with the positive phase aligned with Northern Hemisphere summer insolation (Fig. 4) (Methods). Such a relationship enhances precessional variability in hydroclimate in the eastern African tropics north of the Equator because both factors contribute to increased rainfall. By contrast, the IOD is out of phase with summer insolation in the Southern Hemisphere, so the two factors have opposite effects on rainfall and thereby weaken precessional influence.

Lake Malawi is close to the present-day boundary of the dipolar African rainfall pattern that falls between tropical eastern Africa and southern Africa (Fig. 1a), with contrasting responses to the IOD. Tierney *et al.*[25] report a multidecadal relationship between eastern African rainfall and a positive IOD that differs from the aforementioned inter-annual pattern, with less rainfall over Lake Malawi and other lakes in the rift valley interior and wetter conditions closer to the eastern African coast and the Horn of Africa. In the Malawi record, precessional variation in precipitation may have been further obscured by changes due to migrations of the precipitation pattern boundary; these would have shifted the Malawi basin between the two IOD rainfall regimes.

Several interacting mechanisms may have contributed to the long-term trend towards a wetter climate in the Lake Malawi basin over the past million years. Aridification in the Horn of Africa has been attributed to Indian Ocean cooling due to the northward displacement

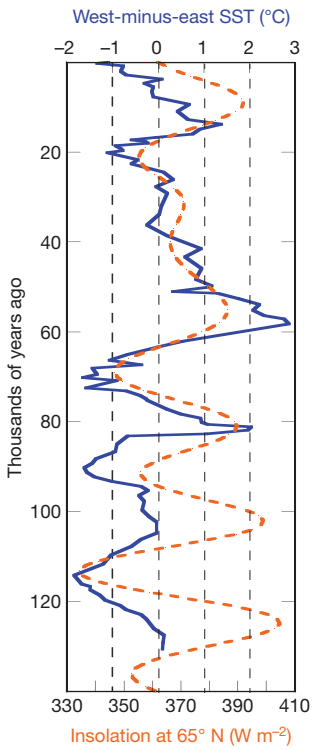

Figure 4 | Northern Hemisphere summer insolation and the Indian Ocean SST gradient. The west-minus-east SST gradient in the equatorial Indian Ocean (IOD) based on alkenone data from two core sites shown in Fig. 1a[29,30] (solid blue line), and Northern Hemisphere (at 65° N) summer insolation (dashed red line) over the past 140,000 years.

of New Guinea and narrowing of the Indonesian throughway over the past 3–4 million years[26]. An overall cooling of the Indian Ocean should result in a drier hydroclimate throughout eastern Africa, even in the Malawi basin. However, an anti-phased relationship in hydroclimate response to the IOD in the interior rift valley versus coastal eastern Africa and the Horn of Africa[25] suggests not only that the Indian Ocean became cooler, but that the IOD became progressively less positive over time. Model results suggest that this would be accompanied by a weakening of a localized Walker circulation over the Indian Ocean, less ascending air over the western Indian Ocean and coastal Africa, and more precipitation in the rift valley, including Lake Malawi[25].

Lake Malawi sediment recorded a transition from a highly variable and predominantly arid climate before 900 kyr ago to a progressively more humid environment after the Mid-Pleistocene Transition, which was dominated by 100-kyr cycles consisting of warm, wet interglacial periods alternating with cooler, drier glacial periods. This shift towards more humid conditions contrasts with the well documented progression towards more aridity in northern Africa over the same period, as recorded in the carbon isotopic composition of soil carbonates and in dust fluxes to sediments in both the Atlantic Ocean and the Gulf of Aden (Extended Data Fig. 3)[2]. Yet another pattern is shown in a leaf-wax isotope record of South African vegetation (recovered from the tropical Atlantic Ocean) that displays a shift in dominant periodicity from about 40-kyr to about 100-kyr cycles through the Mid-Pleistocene Transition[27], as observed in the Malawi record, but with no long-term trend towards either wetter or drier conditions. This growing body of evidence attests to a large regional variability in climate history over the African continent.

Regional differences in hydroclimate undoubtedly influenced the migration of our human ancestors[28]. As northern Africa became more arid over the past million years, the Malawi basin evolved towards a wetter, more hospitable environment, at least during interglacial times. The Malawi record raises key questions about African climate, regarding how much of the rift valley shifted to wetter conditions over the past million years, whether MIS 14 was an unusually cold ice age throughout the region, and what role precessional forcing had on hydroclimate to the north of Malawi. Future drilling campaigns on the East African Great Lakes will offer unique opportunities to address these questions and to understand the changing landscape where our ancestors evolved, migrated and advanced their cultures.

Online Content Methods, along with any additional Extended Data display items and Source Data, are available in the online version of the paper; references unique to these sections appear only in the online paper.

Received 10 December 2015; accepted 28 June 2016.
Published online 10 August 2016.

1. Cerling, T. E. Development of grasslands, savannas in East Africa during the Neogene. *Palaeogeogr. Palaeoclimatol. Palaeoecol.* **97,** 241–247 (1992).
2. deMenocal, P. African climate change and faunal evolution during the Pliocene-Pleistocene. *Earth Planet. Sci. Lett.* **220,** 3–24 (2004).
3. Potts, R. Evolution and climate variability. *Science* **273,** 922–923 (1996).
4. Otto-Bliesner, B. *et al.* Coherent changes of southeastern equatorial and northern African rainfall during the last deglaciation. *Science* **346,** 1223–1227 (2014).
5. Trauth, M. H., Maslin, M. A., Deino, A. & Strecker, M. R. Late Cenozoic moisture history of East Africa. *Science* **309,** 2051–2053 (2005).
6. Liesecki, L. E. & Raymo, M. E. A Pliocene-Pleistocene stack of 57 globally distributed benthic $\delta^{18}O$ records. *Paleoceanography* **20,** PA1003 (2004).
7. Lüthi, D. *et al.* High-resolution carbon dioxide concentration record 650,000–800,000 years before present. *Nature* **453,** 379–382 (2008).
8. Finney, B. P., Scholz, C. A., Johnson, T. C., Trumbore, S. & Southon, J. in *The Limnology, Climatology, and Palaeoclimatology of the East African Lakes* (eds Johnson, T. C. & Odada, E. O.) 495–508 (Gordon and Breach, 1996).
9. Scholz, C. A. *et al.* East African megadroughts between 135–75 kyr ago and implications for early human history. *Proc. Natl Acad. Sci. USA* **104,** 16416–16421 (2007).
10. Pearson, A. & Ingalls, A. E. Assessing the use of archaeal lipids as marine environmental proxies. *Annu. Rev. Earth Planet. Sci.* **41,** 359–384 (2013).
11. Schouten, S., Hopmans, E. C. & Sinninghe Damsté, J. S. The organic geochemistry of glycerol dialkyl glycerol tetraether lipids: a review. *Org. Geochem.* **54,** 19–61 (2013).
12. Winckler, G., Anderson, R. F., Fleisher, M. Q., McGee, D. & Mahowald, N. Covariant glacial–interglacial dust fluxes in the equatorial Pacific and Antarctica. *Science* **320,** 93–96 (2008).
13. Albani, S. *et al.* Improved dust representation in the Community Atmosphere Model. *J. Adv. Model. Earth Syst.* **6,** 541–570 (2014).
14. Lyons, R. P. *et al.* A continuous 1.3 million year record of East African hydroclimate, and implications for patterns of evolution and biodiversity. *Proc. Natl Acad. Sci.* **112,** 15568–15573 (2015).
15. Lyons, R. P., Scholz, C. A., Buoniconti, M. R. & Martin, M. R. Late Quaternary stratigraphic analysis of the Lake Malawi Rift, East Africa: an integration of drill-core and seismic-reflection data. *Palaeogeogr. Palaeoclimatol. Palaeoecol.* **303,** 20–37 (2011).
16. Magill, C. R., Ashley, G. M. & Freeman, K. H. Ecosystem variability and early human habitats in eastern Africa. *Proc. Natl Acad. Sci. USA* **110,** 1167–1174 (2013).
17. Cerling, T. E. *et al.* Woody cover and hominin environments in the past 6 million years. *Nature* **476,** 51–56 (2011).
18. Cohen, A. S. *et al.* Ecological consequences of early Late Pleistocene megadroughts in tropical Africa. *Proc. Natl Acad. Sci.* **104,** 16422–16427 (2007).
19. deMenocal, P. *et al.* Abrupt onset and termination of the African Humid Period: rapid climate responses to gradual insolation forcing. *Quat. Sci. Rev.* **19,** 347–361 (2000).
20. Finney, B. P. & Johnson, T. C. Sedimentation in Lake Malawi (East Africa) during the past 10,000 years: a continuous paleoclimate record from the southern tropics. *Palaeogeogr. Palaeoclimatol. Palaeoecol.* **85,** 351–366 (1991).
21. Van Bocxlaer, B., Salenbien, W., Praet, N. & Verniers, J. Stratigraphy and paleoenvironments of the early to middle Holocene Chipalamawamba Beds (Malawi, Africa). *Biogeosciences* **9,** 4497–4512 (2012).
22. Burrough, S. L., Thomas, D. S. G. & Bailey, R. M. Mega-lake in the Kalahari: a Late Pleistocene record of the paleolake Makgadikgadi system. *Quat. Sci. Rev.* **28,** 1392–1411 (2009).
23. Thomas, D. S. G., Bailey, R., Shaw, P. A., Durcan, J. A. & Singrayer, J. S. Late Quaternary highstands at Lake Chilwa, Malawi: frequency, timing and possible forcing mechanisms in the last 44 ka. *Quat. Sci. Rev.* **28,** 526–539 (2009).
24. Goddard, L. & Graham, N. E. Importance of the Indian Ocean for simulating rainfall anomalies over eastern and southern Africa. *J. Geophys. Res.* **104,** 19099–19116 (1999).
25. Tierney, J. E., Smerdon, J. E., Anchukaitis, K. J. & Seager, R. Multidecadal variability in East African hydroclimate controlled by the Indian Ocean. *Nature* **493,** 389–392 (2013).
26. Cane, M. A. & Molnar, P. Closing of the Indonesian seaway as a precursor to east African arifidication around 3–4 million years ago. *Nature* **411,** 157–162 (2001).

27. Schefuß, E., Schouten, S., Jansen, J. H. F. & Sinninghe Damsté, J. S. African vegetation controlled by tropical sea surface temperatures in the mid-Pleistocene period. *Nature* **422,** 418–421 (2003).
28. Trauth, M. H. *et al.* High- and low-latitude forcing of Plio-Pleistocene East African climate and human evolution. *J. Hum. Evol.* **53,** 475–486 (2007).
29. Mohtadi, M. *et al.* IGBP PAGES, https://www.ncdc.noaa.gov/cdo/f?p=519:1:0::::P1_STUDY_ID:19139 (NOAA World Data Center for Paleoclimatology, 2011).
30. Bard, E., Rostek, F. & Sonzogni, C. Interhemispheric synchrony of the last deglaciation inferred from alkenone palaeothermometry. *Nature* **385,** 707–710 (1997).

Supplementary Information is available in the online version of the paper.

Acknowledgements We thank the engineering and design team of the Lake Malawi Scientific Drilling Project for overcoming substantial technical challenges associated with drilling on Lake Malawi, especially the efforts of D. Schnurrenberger, M. Pardy and Lengeek Vessel Engineering. B. Otto-Bliesner and S. Albani provided advice on climate model results relevant to this study. J. King provided the palaeomagnetic reversal data that contributed substantially to the age model of the Malawi sediment record. We thank the scientists and technicians of LacCore, University of Minnesota, for their assistance in the splitting, initial analyses, sampling and archiving of the sediment cores obtained by the Lake Malawi Drilling Project. Financial support was provided by the US National Science Foundation EAR and P2C2 programmes and by the International Continental Scientific Drilling Program. S.S. and J.S.S.D. were supported by the Netherlands Earth System Science Centre (NESSC), which is financially supported by the Dutch Ministry of Education, Culture and Science (OCW).

Author Contributions T.C.J., J.P.W. and E.T.B. conceptualized the project. C.A.S. and T.C.J. were two of the Principal Investigators on the Lake Malawi Drilling Project. J.P.W., J.S.S.D. and S.S. supervised and interpreted the biomarker analyses conducted by A.A., M.B., J.H., S.C. and S.G. E.T.B. supervised the X-ray fluorescence analyses for calcium. A.D. provided Ar–Ar dates on tephra. R.P.L. provided the lake level history. B.A.S. conducted the statistical analyses. T.C.J. and E.T.B. wrote the manuscript with substantial contributions from J.P.W., A.A., M.B., B.A.S., S.C., S.S. and J.S.S.D. All authors reviewed the paper prior to submission.

Author Information The data used in this study are available as Supplementary Data. Reprints and permissions information is available at www.nature.com/reprints. The authors declare no competing financial interests. Readers are welcome to comment on the online version of the paper. Correspondence and requests for materials should be addressed to T.C.J. (tcj@d.umn.edu).

Reviewer Information *Nature* thanks K. Freeman, P. Polissar and the other anonymous reviewer(s) for their contribution to the peer review of this work.

METHODS

The Lake Malawi Drilling Project recovered a 380-m sediment sequence in 2005 from a water depth of 590 m. Cores MAL05-1B and MAL05-1C of the Drilling Project, and a nearby piston core M98-13P (Extended Data Table 1) were analysed for past temperature and rainfall. Seismic reflection profiles used to select the site portray an undisturbed sedimentary section that was not impacted by erosion, turbidity currents or mass wasting events[15]. Sediment samples were analysed to produce records of temperature (TEX_{86}) and aridity (calcium content and leaf wax $\delta^{13}C$).

Palaeo-temperature derived from TEX_{86}. TEX_{86} is a proxy for temperature in the upper water column, based on the distribution of glycerol dialkyl glycerol tetraether (GDGT) membrane lipids of *Thaumarchaeota* living in the water column[31,32]. *Thaumarchaeota* are ammonia oxidizers that live throughout the aerobic and suboxic water column, but have been found in many lake systems to have a maximum abundance just below the thermocline or chlorophyll maximum[33,34]. Indeed, in Lake Malawi the maximum abundance of the most labile GDGT produced by Thaumarchaea has been identified at 50 m water depth[34]. Nevertheless, the distribution of their lipids is strongly related to surface water temperature in many lake systems[31,35,36]. The GDGTs used to determine TEX_{86} are well preserved in sediments and have been identified intact in sediments as far back as the Cretaceous Period to estimate past ocean temperatures[37].

Lipids were extracted from 577 freeze-dried, homogenized sediment samples using accelerated solvent extraction (Dionex ASE) using hexane/dichloromethane (DCM) 9:1 (v/v) at 100 °C and 7.6×10^6 Pa to obtain a total lipid extract. The total lipid extract was then separated into neutral, free fatty acid, and phospholipid fatty acid fractions using an aminopropylsilyl bond elute column, cleaned before use with 10 ml successive rinses of methanol followed by 1:1 DCM:2-propanol. Eight millilitres each of 1:1 DCM:2-propanol, 4% glacial acetic acid in distilled ethyl ether, and methanol were used with the cleaned columns to elute the neutral, free fatty acid, and phospholipid fatty acid fractions, respectively. Short column chromatography with activated alumina as the stationary phase was used to further separate the neutral fraction into apolar and polar fractions using 9:1 hexane:DCM followed by 1:1 DCM: methanol as eluents for the two fractions, respectively. The polar fraction containing the GDGT lipids required for TEX_{86} analysis was filtered (0.45 μm filter), dried under N_2, and then redissolved in 99:1 hexane:isopropanol for analysis. The apolar fraction containing *n*-alkanes was further separated into saturated and unsaturated hydrocarbons using Ag^+-impregnated silica gel column chromatography as described in ref. 38.

GDGTs were analysed by high-performance liquid chromatography/atmospheric pressure chemical ionization mass spectrometry (HPLC/APCI-MS), using an Agilent 1100 series liquid chromatograph with an Alltech Prevail Cyano column (150 mm × 2.1 mm; 3 μm diameter)[39]. Annual lake surface temperatures (ALST) in degrees Celsius were calculated using the TEX_{86} ratio of GDGTs[40] and the lake sediment calibration of ref. 41:

$$\mathrm{ALST} = 49.032(\mathrm{TEX}_{86}) - 10.989 \ (r^2 = 0.88;\ n = 16)$$

A global marine calibration for TEX_{86} yields a mean error of 2.5 °C (ref. 42), and the global lake calibration yields a mean error of 3.6 °C (ref. 41). Although this is quite large relative to the rather small interannual variation in tropical temperature, the error of the global calibration is undoubtedly amplified by the differing composition of communities as well as differences in seasonality and depth habitat of *Thaumarchaeota* in different lakes. Within a single lake community, we suspect that the correlation between TEX_{86} and ALST is much tighter.

The sampling interval for TEX_{86} analyses averaged about 10 cm in the depth interval of 0–8 metres below lake floor (m.b.l.f.), 50 cm in the depth interval 8–18 m.b.l.f., and 1 m in the depth interval 18–379 m.b.l.f. Roughly 10% of the samples were run in duplicate, and displayed average differences in TEX_{86} of 0.0076, corresponding to a 2σ temperature value of 0.8 °C.

Acceptance criteria for TEX_{86} data. Palaeotemperature data derived from TEX_{86} analysis may be compromised if the concentrations of the isomers used to calculate TEX_{86} are too low, or if a substantial portion of the isoprenoid GDGTs used to calculate TEX_{86} are derived from sources other than *Thaumarchaeota*, such as soil archaea in the catchment or methanogenic archaea living in the lower water column[43]. We accepted TEX_{86} values for our palaeotemperature reconstructions as long as the following criteria were met:

(1) The signal must be above the limit of quantitation[39], which in our case corresponded to integral peak areas $>10^4$ for the 1,300 and 1,292 ('cren') isomers.

(2) The ratio of GDGT-0/crenarchaeol <2.0 must exclude the impact of methanogen archaea.

(3) The crenarchaeol isomer must be $<10\%$ of the sum of the crenarchaeol and the crenarchaeol isomer and GDGT-2 must be $<45\%$ of the total GDGTs to exclude influences of archaea other than *Thaumarchaeota*.

(4) The BIT (branched and isoprenoid tetraether) index must be >0.5 to exclude the impact of soil-derived GDGTs (see refs 11 and 43 for further explanation and rationale for these criteria).

Using these criteria, we rejected 107 of the 584 analyses for TEX_{86}. The rejected TEX_{86} data yielded temperatures ranging between about 4 °C and 38 °C. Nearly all of them were associated with a BIT index >0.5, and most were warmer than adjacent temperatures that met our acceptance criteria (Extended Data Fig. 4). The temperatures derived from the accepted TEX_{86} measurements fall within a range of ~18–28 °C (Extended Data Fig. 4).

Almost all of the TEX_{86} values that were rejected correlate with depths where the sediments are calcareous and a lake-level index based on sediment composition[14] indicates relatively arid conditions with the lake at a lowstand. Under such conditions, the shoreline would have encroached upon the drill site, increasing the likelihood of terrestrially derived GDGT input from the catchment, a diminished aquatic production of GDGTs by *Thaumarchaeota*, proliferation of other archaeal species, and potential remobilization of previously deposited shallower water sediments.

Temperature correction due to changing lake-surface elevation. The remaining accepted temperatures were then corrected for the lapse rate effect of the lake's major lowstands. Lake Malawi has experienced drops of several hundred metres in lake level during prolonged arid periods in the past (referred to as "megadroughts" in ref. 9), and during such times of depressed lake level, water temperature would have risen owing to the temperature lapse rate alone, independent of any regional change in temperature. The lake-level history is not known precisely, but is best represented by principal component 1 (Lyons' PC1, or LPC1)[14], derived from principal component analysis of four sediment parameters: natural gamma radiation, C/N ratio and $\delta^{13}C$ of bulk organic matter, and reflected colour of the core digital image. We corrected the TEX_{86} temperatures by using the linear relationship between LPC1 and lake-level depression (in metres) that Lyons *et al.*[14] derived from direct comparison of LPC1 with the depths of correlative lowstand deltas identified on seismic reflection profiles:

$$\Delta\mathrm{LL} = -154.18(\mathrm{LPC1}) - 247.05 \ (R^2 = 0.9628)$$

where ΔLL is the drop in lake level, in metres, from the present-day lake level.

Assuming a moist tropical lapse rate of 6 °C km^{-1}, we multiplied negative values of ΔLL by 0.006 to obtain the temperature correction to be subtracted from the original TEX_{86} temperature to arrive at a temperature for constant lake elevation. In the few intervals where ΔLL had a positive value (implying lake level higher than the present lake level), no temperature correction was applied because the lake cannot rise much above outlet elevation, and the lapse rate effect would be negligible. We applied the prediction uncertainty range of the Lyons *et al.*[14] PC1-to-lake-level relationship to estimate uncertainty in the lapse-rate-based temperature correction. The positive 2σ prediction uncertainty values were adjusted to not exceed a lake-surface elevation change ΔLL of greater than zero (that is, during times of high lake level and overflow). The overall temperature uncertainty was calculated by adding in quadrature the analytical (2σ of 0.8 °C, described above) and lapse-rate correction uncertainties and resulted in average and maximum 2σ values of about 1.0 °C and 1.3 °C, respectively. The correction for lapse rate effect reduces the average temperature of the record by about 2 °C, but the overall amplitude of temperature shift and the occurrence of distinct intervals of relatively warm and relatively cold temperatures remain (Extended Data Fig. 1).

Palaeo-aridity derived from $\delta^{13}C$ of leaf-wax *n*-alkanes and calcium abundance. Stable carbon isotopic compositions of C_{29}–C_{33} *n*-alkanes derived from fossil leaf waxes primarily reflect the relative abundances of C_3 (mostly trees, shrubs and herbs) and C_4 (mostly grass) vegetation[16,32]. An Agilent 6890N gas chromatograph (60-m HP-1 column, 0.32 mm inner diameter, 0.25 μm film thickness) interfaced to a Thermo Finnigan Delta^{Plus} XP mass spectrometer via a combustion interface was used to determine the $\delta^{13}C$ of *n*-alkanes. All $\delta^{13}C$ values are reported as per mil deviations from the Vienna Pee Dee Belemnite (VPDB) standard using conventional delta notation. The gas chromatograph temperature program begins at 50 °C and increases at a rate of 50 °C min^{-1} to 180 °C and next at a rate of 3 °C min^{-1} to 320 °C. The final temperature of 320 °C is held for 6 min. The *n*-alkanes separated by the gas chromatography column are oxidized at 940 °C and converted to carbon dioxide. A standard mixture of *n*-alkanes of known $\delta^{13}C$ values was analysed multiple times daily ('Mix-A' of C_{16}–C_{30} *n*-alkanes provided by A. Schimmelmann, Indiana University); from these replicate measurements, the typical precision of the $\delta^{13}C$ measurements is ±0.5‰ (1σ). Each sample was run at least in duplicate and co-injected with squalane as an internal standard to monitor reproducibility of measurements. Replicates were analysed and plotted individually for each *n*-alkane sample, with a mean error of ±0.41‰ for C_{31} duplicates.

While C_3 herbs are found in both woodlands and grasslands, $\delta^{13}C$ of C_{31} *n*-alkanes in tropical eastern Africa generally reflect the restructuring of the landscape between woodlands dominated by C_3 vegetation, indicating relatively humid conditions, and by C_4 grasslands, representing relatively arid conditions in the lake basin[16].

The trends of $\delta^{13}C$ in the C_{29}, C_{31}, and C_{33} *n*-alkanes are broadly similar in timing and amplitude (Extended Data Fig. 5). Any one of these profiles could have been used to reflect the history of vegetation and hydroclimate on the landscape surrounding Lake Malawi, and would have been consistent with our interpretation of the environmental history of the region. We chose to reflect the terrigenous leaf-wax data as $\delta^{13}C_{31}$, which is usually the most abundant of the three *n*-alkanes and was chosen by ref. 16 to relate to C_3 and C_4 plant-type abundance in eastern Africa, which we utilize in Fig. 2. We find the down-core trend in $\delta^{13}C_{31}$ to closely track the trend in $\delta^{13}C_{wax}$, the weighted mean average of the three *n*-alkanes that has been reported in previous studies in eastern Africa (see ref. 38) (Extended Data Fig. 5).

Calcium abundance in bulk sediment, determined by scanning X-ray fluorescence, was used as another indicator of past hydroclimate. The calcium signal is strongly bi-modal, exhibiting high values in calcareous sediments, which accumulate only during lake lowstands[20,44] and low values during wetter conditions when the lake overflows at its outlet, leaving the water column under-saturated with respect to calcite[45].

Refining the age model for the MAL05-1 drilling site. Our age model (Fig. 1c) is based initially on 15 radiocarbon dates in the upper 16 m of core, the presence of the youngest Toba ash (75 ± 1 kyr ago) at 28.1 m.b.l.f. (ref. 46), Ar–Ar dates on tephra at 167.8 m.b.l.f. (590 ± 20 kyr ago) and 241.6 m.b.l.f. (915 ± 8 kyr ago), and six palaeomagnetic reversals beginning with the Brunhes–Matuyama at 222 m.b.l.f. (ref. 14) (Extended Data Fig. 6a, Extended Data Table 2). These dates indicate an average sedimentation rate of 0.28 m kyr^{-1} for the drill site, although they provide no age control in the interval between 75 kyr ago (Toba ash horizon) and 590 kyr ago (the younger of the two Ar–Ar dates). The corrected temperature versus depth-in-core record (Extended Data Fig. 1b) displays a statistically significant 33.6-m cycle, which corresponds to an eccentricity period of about 121 kyr, assuming a sedimentation rate of about 0.28 m kyr^{-1} (see statistics in Extended Data Fig. 6b). We note that the raw temperature data before correction for lapse rate also displays a significant cycle of 38.5 m (bandwidth is 0.0001 and 80% error estimate on the power spectrum is 0.626), which indicates that the lapse rate correction is not artificially introducing cyclicity into the temperature record. Consequently, we align the TEX_{86} corrected temperature record with the LR04 marine stacked benthic foraminiferal $\delta^{18}O$ record to assign ages in the interval 75–590 kyr ago, recognizing that the periods of relatively warm temperature must have coincided with interglacials and relatively cool temperatures with glacial periods (Extended Data Fig. 6c). The resultant age assignments and sedimentation rates based on this alignment do not deviate dramatically from the initial age model (Extended Data Fig. 6a).

Employing our age model, we performed Blackman–Tukey spectral analysis on the lake-level history derived from LPC1 (Extended Data Fig. 2). A strong spectral peak corresponding to an approximately 100-kyr (eccentricity) cycle appears for the period from 900 kyr ago to the present, but not before 900 kyr ago. We conclude that: (1) the tuned age model is credible, and (2) a statistically significant shift to 100 kyr cycles in climate variability occurred at about 900 kyr ago (see statistics in Extended Data Fig. 2).

Calculating the IOD for the past 130 kyr. We examined variation in the IOD on a timescale of 10^4–10^5 years by subtracting a 130-kyr alkenone record of SST in the eastern Indian Ocean (core GeoB 10038-4: 5° 56.25′ S, 103° 14.76′ E; ref. 29) from an alkenone SST record in the western Indian Ocean (core MD85668: 0° 01′ N, 46° 02′ E; ref. 30) (Extended Data Fig. 7).

31. Powers, L. A. *et al.* Applicability and calibration of the TEX_{86} paleothermometer in lakes. *Org. Geochem.* **41,** 404–413 (2010).
32. Castañeda, I. S. & Schouten, S. A review of molecular organic proxies for examining modern and ancient lacustrine environments. *Quat. Sci. Rev.* **30,** 2851–2891 (2011).
33. Woltering, M. L. *et al.* Vertical and temporal variability in concentration and distribution of thaumarchaeotal tetraether lipids in Lake Superior and the implications for the application of the TEX_{86} temperature proxy. *Geochim. Cosmochim. Acta* **87,** 136–153 (2012).
34. Woltering, M. L. *Thaumarchaeota Distribution in the Water Column of Lake Superior and Malawi: Implications for the TEX86 Temperature Proxy*. http://gradworks.umi.com/34/82/3482290.html, PhD thesis, Univ. Minnesota (2011).
35. Blaga, C. I., Reichart, G.-J., Lotter, A. F., Anselmetti, F. S. & Sinninghe Damsté, J. S. A TEX_{86} lake record suggests simultaneous shifts in temperature in central Europe and Greenland during the last deglaciation. *Geophys. Res. Lett.* **40,** 948–953 (2013).
36. Blaga, C. I. *et al.* Seasonal changes in glycerol dialkyl glycerol tetraether concentrations and fluxes in a perialpine lake: implications for the use of the TEX_{86} and BIT proxies. *Geochim. Cosmochim. Acta* **75,** 6416–6428 (2011).
37. Schouten, S. *et al.* Extremely high sea-surface temperatures at low latitutudes during the middle Cretaceous as revealed by archaeal membrane lipids. *Geology* **31,** 1069–1072 (2003).
38. Castañeda, I. S., Werne, J. & Johnson, T. C. Wet and arid phases in the southeast African tropics since the Last Glacial Maximum. *Geology* **35,** 823–826 (2007).
39. Schouten, S., Huguet, C., Hopmans, E. C., Kienhuis, M. V. M. & Sinninghe Damsté, J. S. Analytical methodology for TEX_{86} paleothermometry by high-performance liquid chromatography/atmospheric pressure chemical ionization-mass spectrometry. *Anal. Chem.* **79,** 2940–2944 (2007).
40. Schouten, S., Hopmans, E. C., Schefuss, E. & Sinninghe Damsté, J. S. Distributional variations in marine crenarchaeotal membrane lipids: a new tool for reconstructing ancient sea water temperatures? *Earth Planet. Sci. Lett.* **204,** 265–274 (2002).
41. Castañeda, I. S. & Schouten, S. Corrigendum to "A review of molecular organic proxies for examining modern and ancient lacustrine environments". *Quat. Sci. Rev.* **125,** 174–176 (2015).
42. Kim, J.-H., Schouten, S., Hopmans, E. C., Donner, B. & Sinninghe Damsté, J. S. Global sediment core-top calibration of the TEX_{86} paleothermometer in the ocean. *Geochim. Cosmochim. Acta* **72,** 1154–1173 (2008).
43. Sinninghe Damsté, J. S., Ossebaar, J., Schouten, S. & Verschuren, D. Distribution of tetraether lipids in the 25-ka sedimentary record of Lake Challa: extracting reliable TEX_{86} and MBT/CBT palaeotemperatures from an equatorial African lake. *Quat. Sci. Rev.* **50,** 43–54 (2012).
44. Brown, E. T. Lake Malawi's response to "megadrought" terminations: sedimentary records of flooding, weathering and erosion. *Palaeogeogr. Palaeoclimatol. Palaeoecol.* **303,** 120–125 (2011).
45. Ricketts, R. D. & Johnson, T. C. in *The Limnology, Climatology and Paleoclimatology of the East African lakes* (eds Johnson, T. C. & Odada, E. O.) 475–493 (Gordon and Breach, 1996).
46. Lane, C., Chorn, B. & Johnson, T. C. Ash from the Toba supereruption in Lake Malawi shows no volcanic winter in East Africa at 75 ka. *Proc. Natl Acad. Sci. USA* **110,** 8025–8029 (2013).
47. Levin, N. E. Environment and climate of early human evolution. *Annu. Rev. Earth Planet. Sci.* **43,** 405–429 (2015).
48. deMenocal, P. B. Plio-Pleistocene African climate. *Science* **270,** 53–59 (1995).

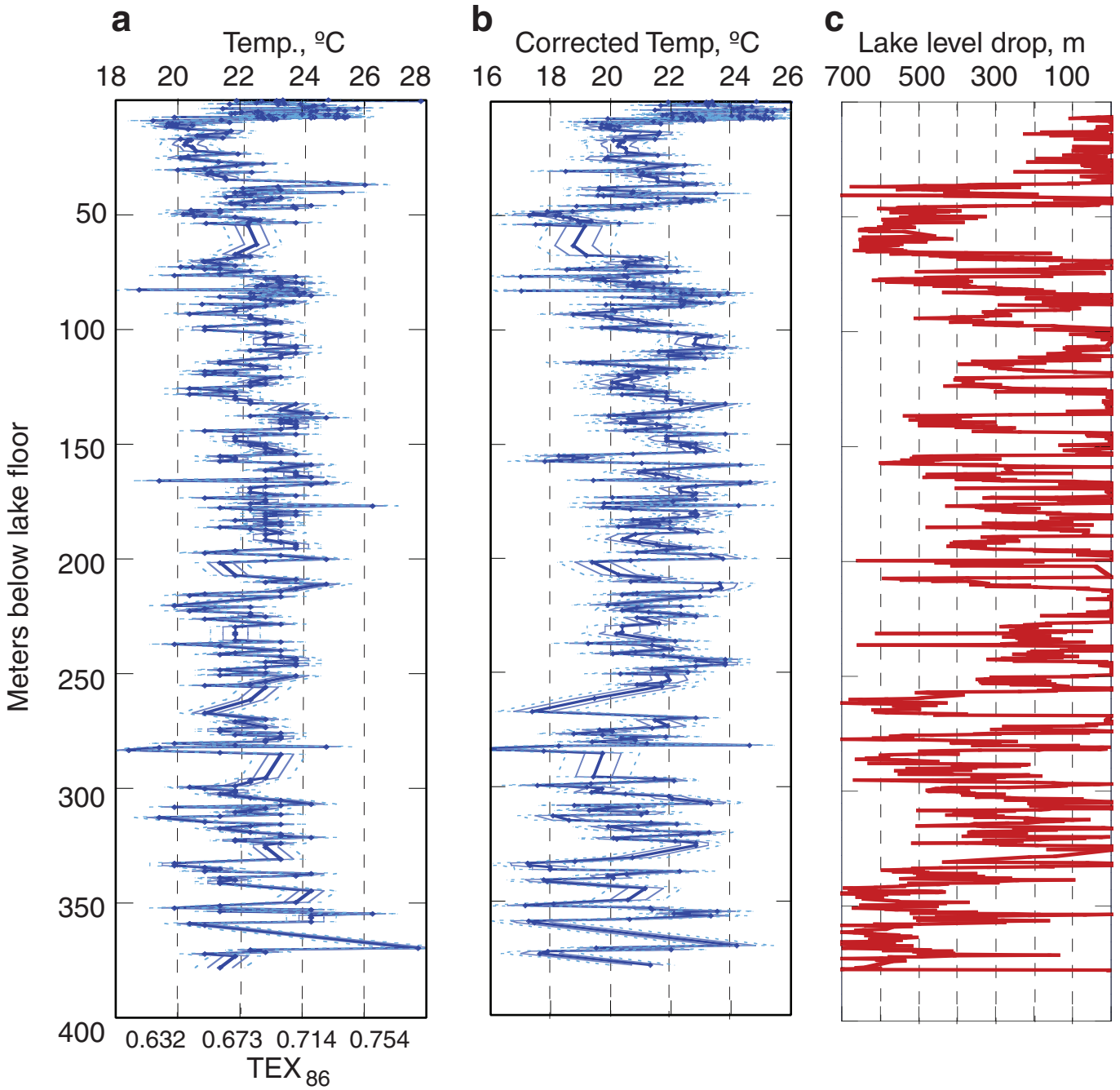

Extended Data Figure 1 | Correcting temperature data for lapse rate effect. a, **b**, Uncorrected TEX_{86} temperature (**a**) and temperature corrected for lapse rate effect (**b**) plotted against burial depth at drilling site MAL05-1. The light solid and dashed lines represent the 1σ and 2σ ranges of uncertainty in both graphs. **c**, Lake-level history, from LPC1[14], which is the basis for the lapse-rate correction to temperature (Methods).

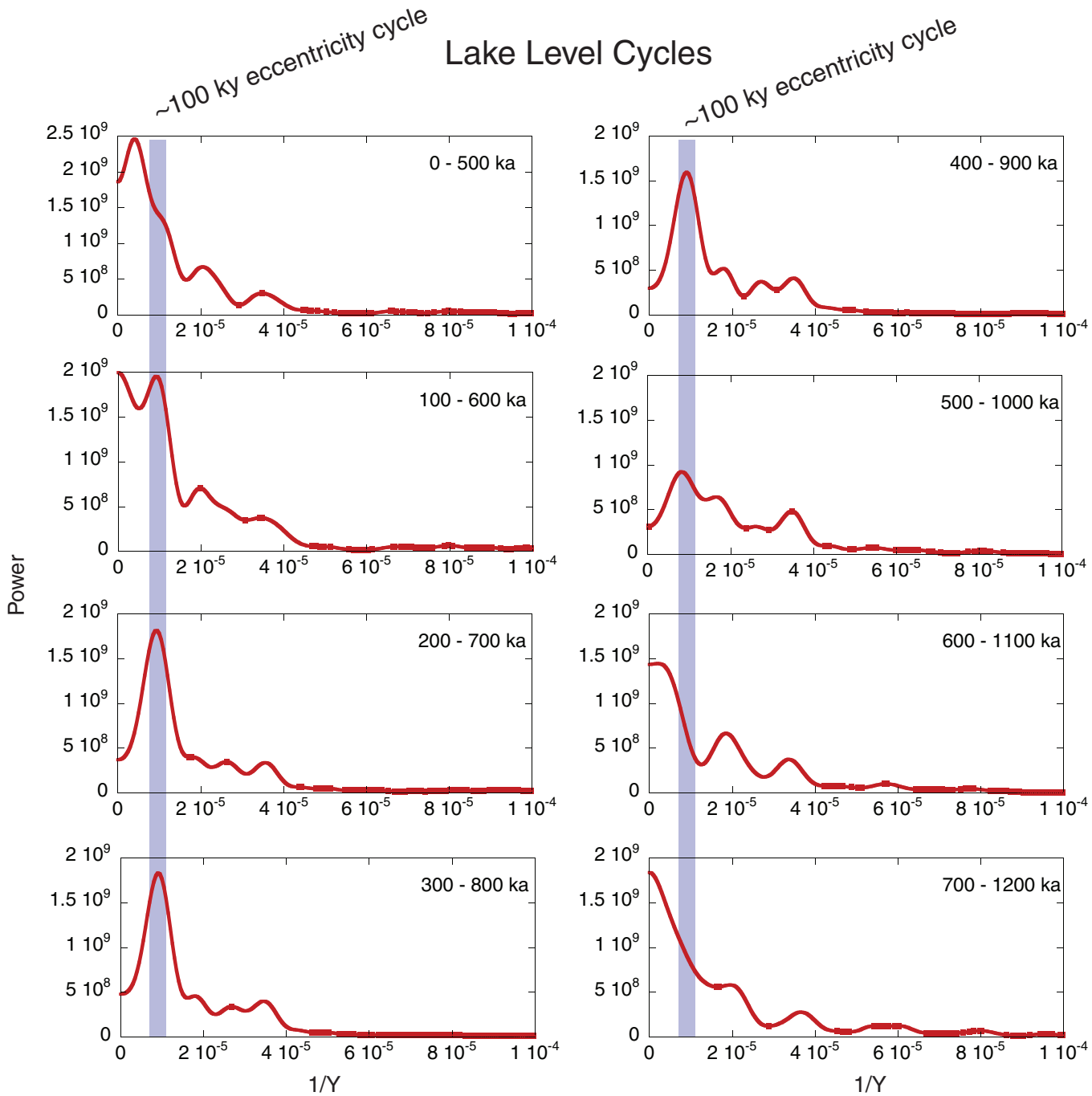

Extended Data Figure 2 | A predominant 100-kyr (eccentricity) cycle in hydroclimate since the Mid-Pleistocene Transition. Blackman–Tukey spectral power versus per year ('1/Y') of 500-kyr intervals from the present back to one million years ago, of the lake-level record portrayed in Extended Data Fig. 1, when dated with the tuned age model depicted in Extended Data Fig. 6. Bandwidth is 0.0001 and the 80% error estimate on the power spectra is 0.626. We note the strong eccentricity cycle back to 900 kyr ago, and its diminishing influence before then. Whereas the temperature record would display this cycle simply because it was tuned to LR04, the lake level record was derived independently of the temperature data[14].

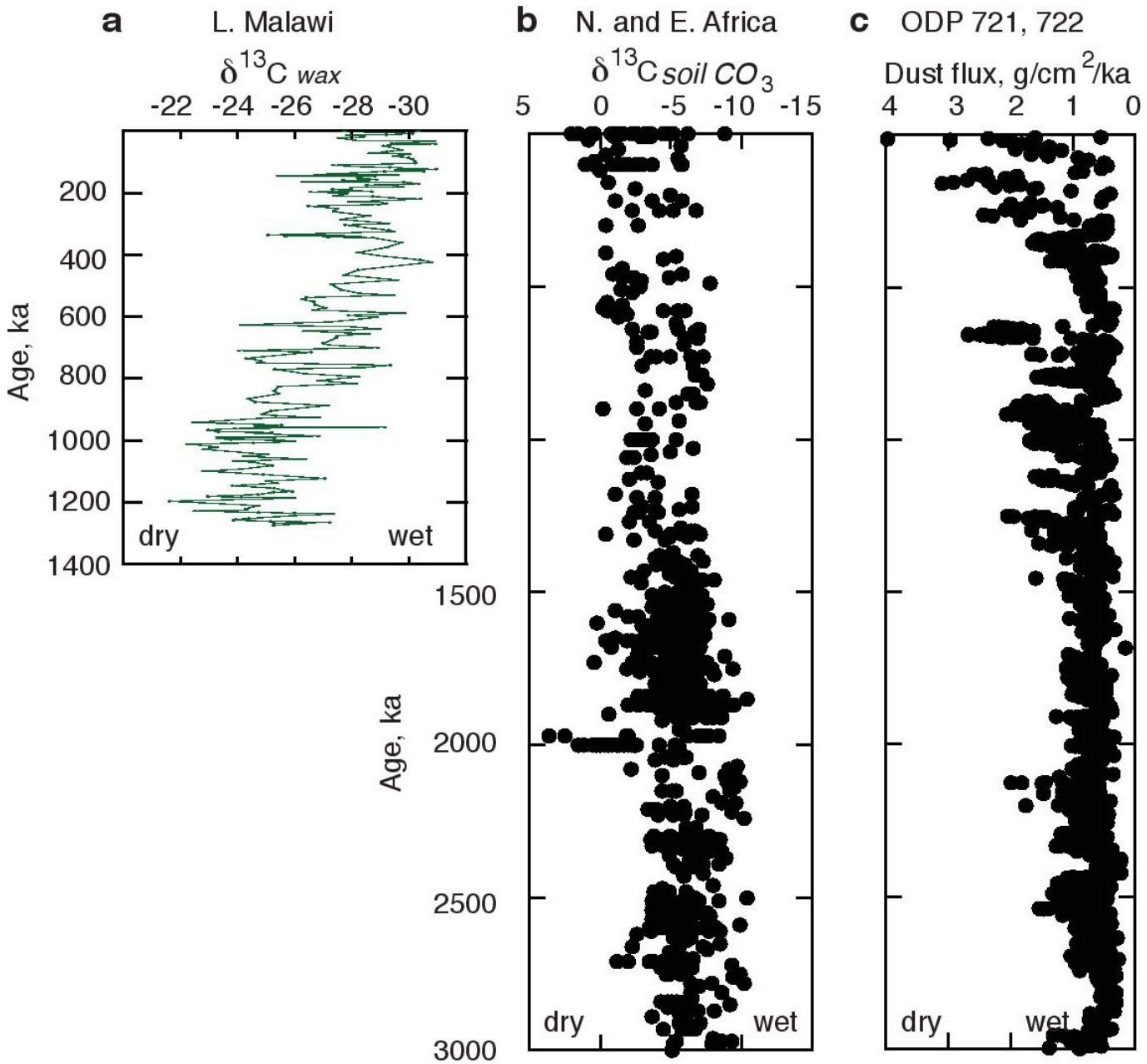

Extended Data Figure 3 | A contrast in hydroclimate history on the African continent. The leaf wax $\delta^{13}C_{31}$ record indicates that the Malawi basin became progressively wetter since the Mid-Pleistocene Transition around 900 kyr ago (**a**), while much of the continent to the north of Lake Malawi maintained a trend towards drier conditions over the past three million years or more, as indicated by soil carbonate $\delta^{13}C$ values in northern Tanzania, Kenya and Ethiopia (summarized in ref. 47) (**b**) and in marine sediment records of terrigenous dust input from northern Africa[48], as shown in ODP Sites 721 and 722 from the Gulf of Aden (**c**).

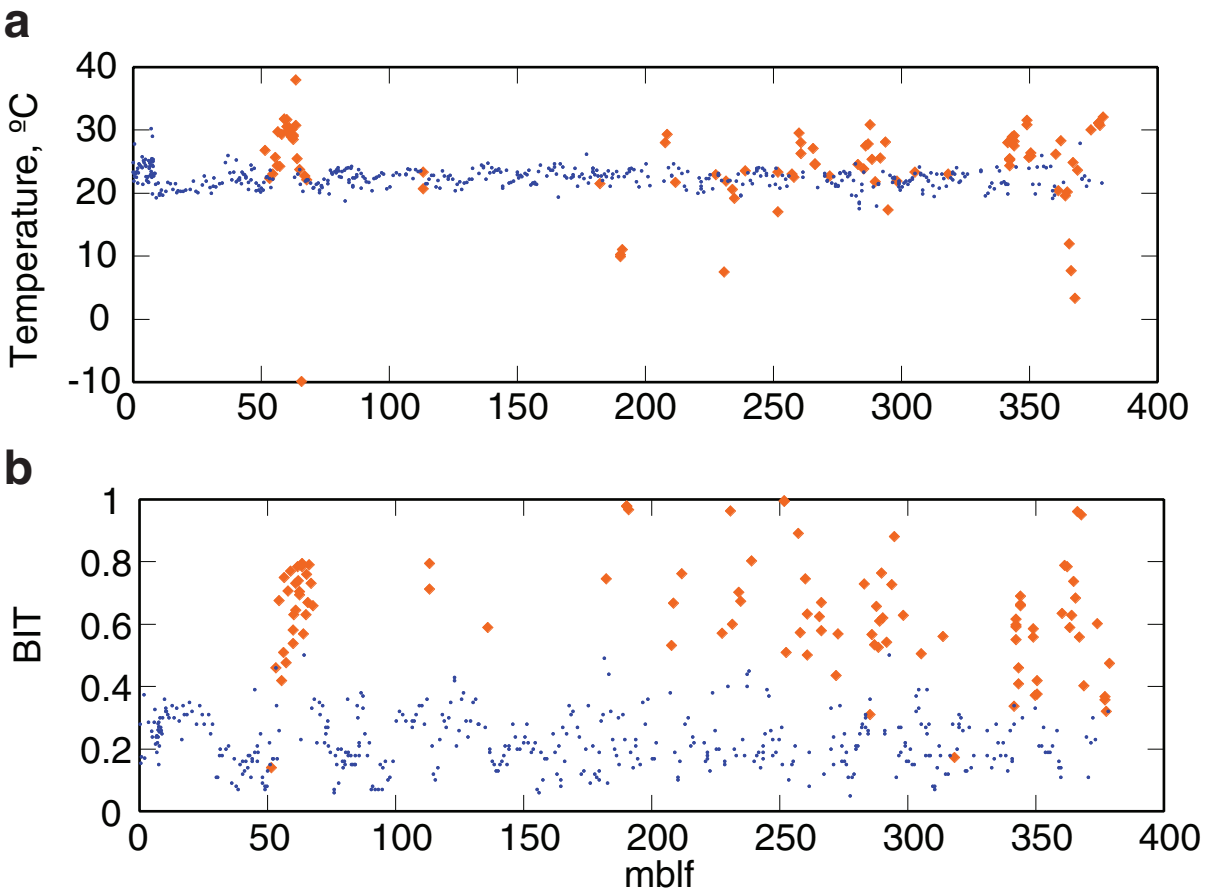

Extended Data Figure 4 | Accepted (blue) and rejected (orange) temperatures and BIT data. Acceptance criteria are explained in the Methods.

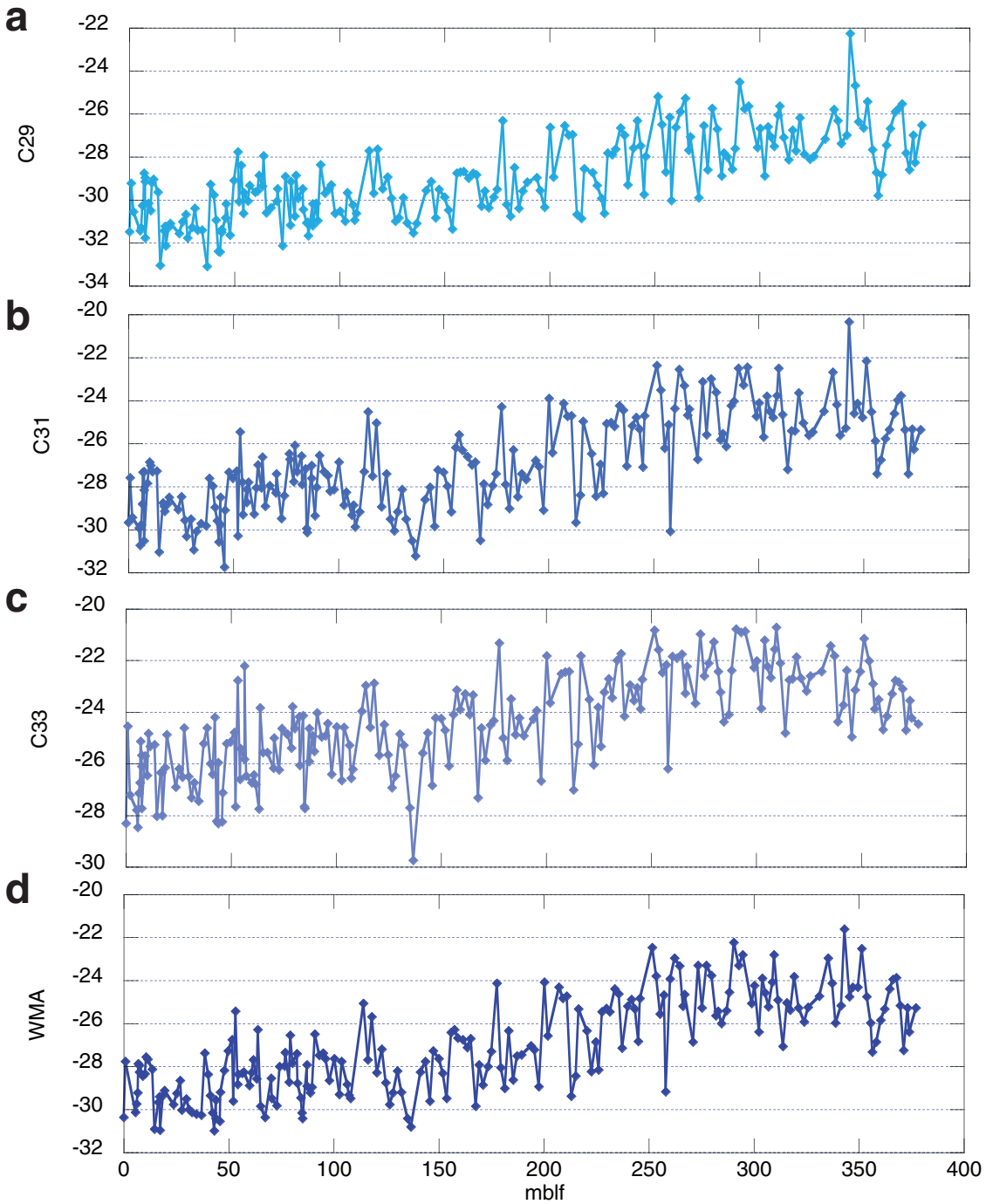

Extended Data Figure 5 | $\delta^{13}C$ of the C_{29}, C_{31}, C_{33} *n*-alkanes. $\delta^{13}C$ of the C_{29}, C_{31} and C_{33} *n*-alkanes (**a**, **b**, **c**), and the weighted mean average (WMA) of these values (**d**).

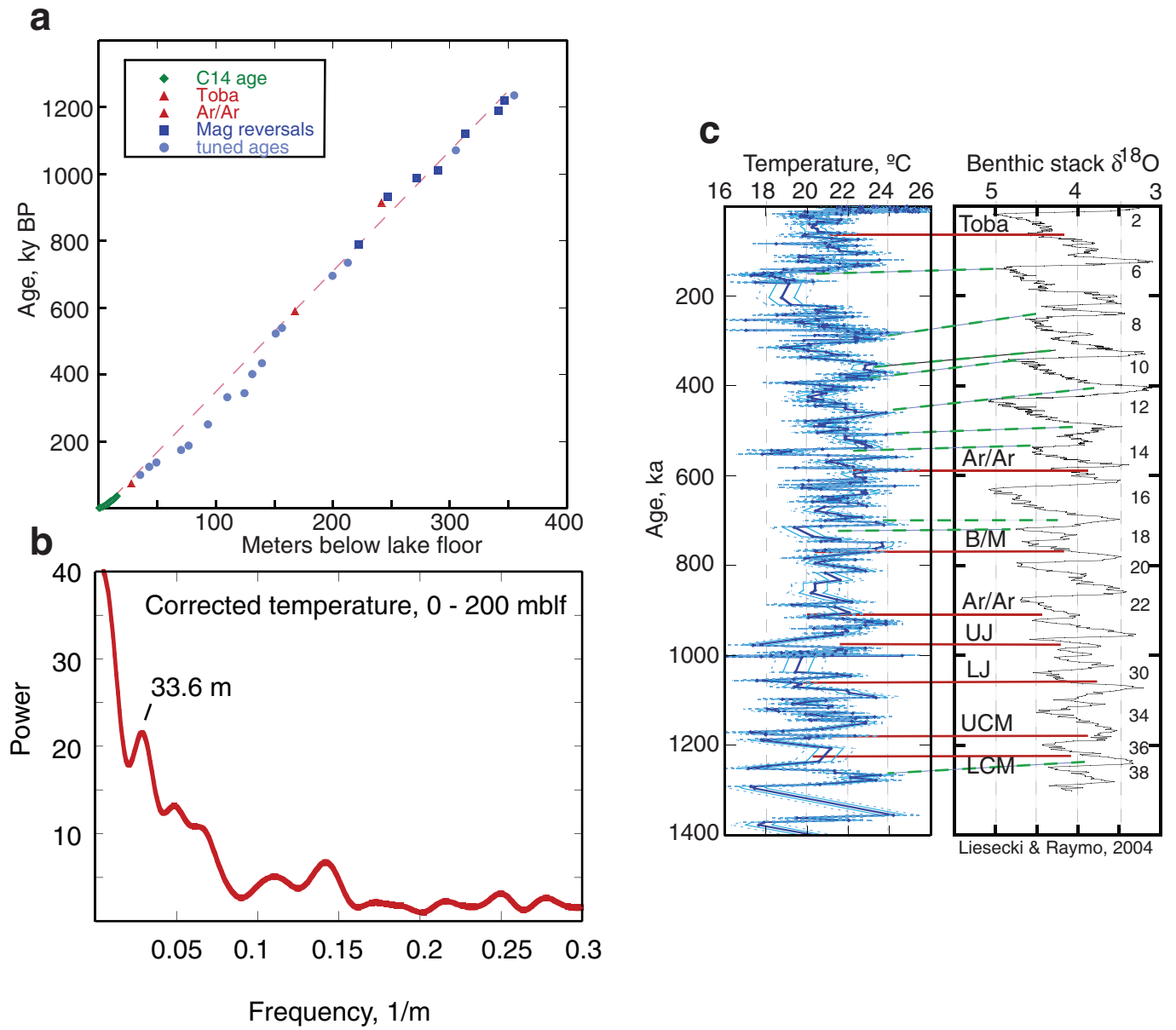

Extended Data Figure 6 | Aligning the temperature record to LR04 to refine the age model. a, Age versus depth for drill site MAL05-1, depicting ages based on ^{14}C, tephra, magnetic reversals and alignment (tuning) of corrected temperature with LR04. The dashed pink line is a linear fit through the dates derived from radiocarbon, tephra and magnetic reversals only, described by the equation: Age (in kyr before present) $= -12.44 + 3.602z$ ($r^2 = 0.9984$). **b**, Blackman–Tukey analysis (spectral power versus per metre) of the corrected temperature data in the upper 200 m of drill site MAL05-1, showing a 33.6-m cycle, which corresponds to about 121 kyr. Bandwidth is 0.0001 and 80% error estimate on the power spectrum is 0.626. **c**, Temperature plotted against age based solely on radiocarbon, tephra and magnetic reversal dates aligned to the LR04 age scale (green dashed lines), in order to assign ages in MAL05-1 between 75 kyr ago (Toba ash horizon) and 590 kyr ago (Ar–Ar). The red lines depict tephra and magnetic reversal ages, which constrain the temperature alignment. B/M, Brunhes–Matuyama; UJ, Upper Jaramillo; LJ, Lower Jaramillo; UCM, Upper Cobb Mountain; LCM, Lower Cobb Mountain. Data are from ref. 14.

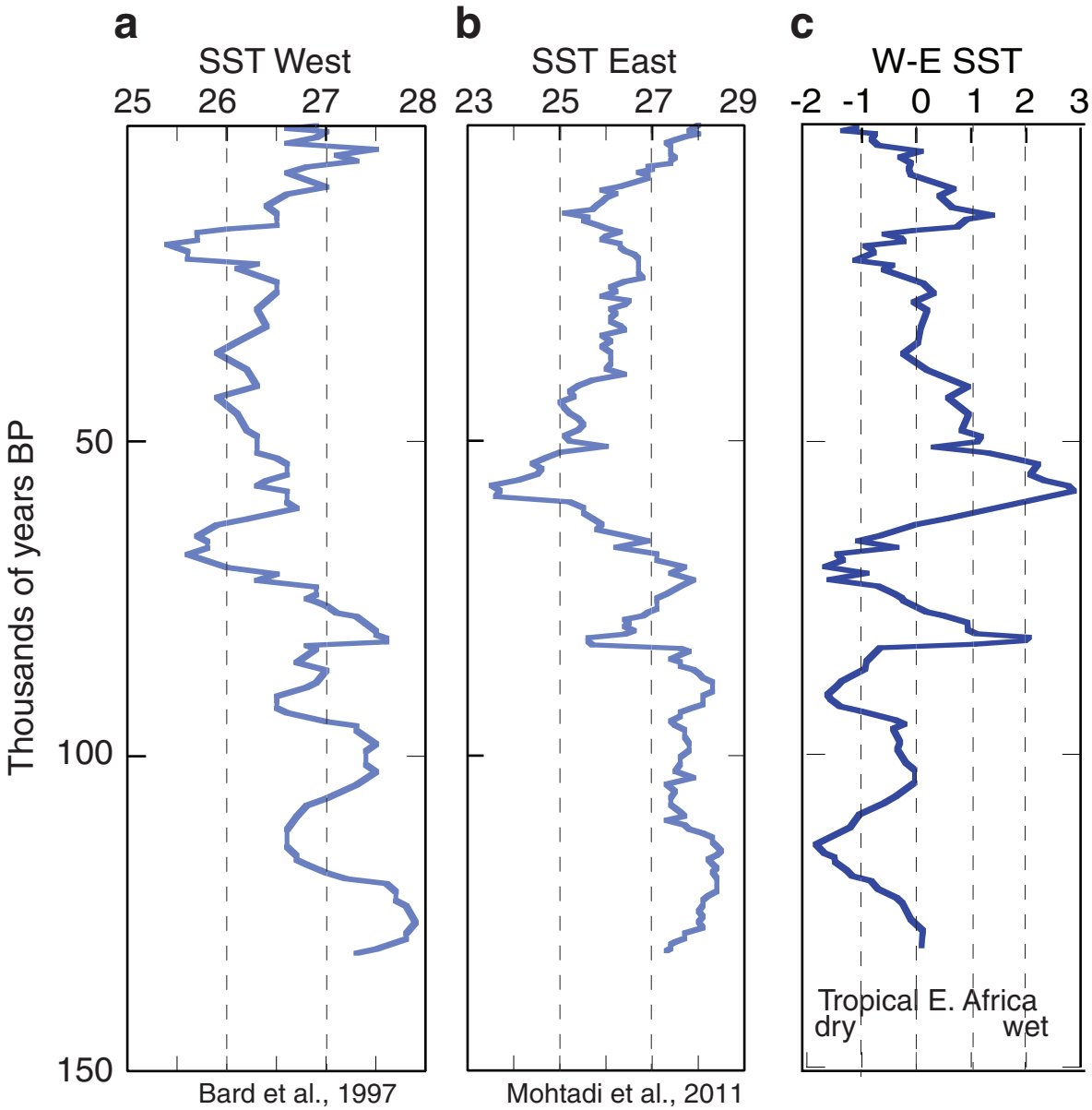

Extended Data Figure 7 | The Indian Ocean west-minus-east gradient in SST since 130 kyr ago. Alkenone records of SST in the western Indian Ocean (core MD85668: 0° 01′ N, 46° 02′ E) (**a**)[30] and the eastern Indian Ocean (core GeoB 10038-4: 5° 56.25′ S, 103° 14.76′ E) (**b**)[29]. The west-minus-east temperature gradient (IOD) derived from these two records is displayed in **c**.

Extended Data Table 1 | Locations of the cores analysed in this study

Site	Latitude	Longitude	Water Depth (m)	Core Length (m)
M98-13P	11º16’ 0” S	34º26’ 6” E	604	8.3
MAL05-1B	11º17’38” S	34º26’14” E	590	379.29
MAL05-1C	11º17’38” S	34º26’14” E	590	88.89

Extended Data Table 2 | Sediment dates that underlie the age model of this study

Meters below lake floor	Cal. Yrs. BP	Age basis
0.555	816	^{14}C
1.70	1770	^{14}C
3.70	4270	^{14}C
5.46	7140	^{14}C
6.71	11010	^{14}C
7.51	12630	^{14}C
7.90	13330	^{14}C
8.51	14565	^{14}C
9.46	18450	^{14}C
9.56	18800	^{14}C
10.55	21530	^{14}C
11.52	23975	^{14}C
12.46	26590	^{14}C
14.09	30890	^{14}C
15.81	36140	^{14}C
28.09	75000	Toba ash
167.84	5.90e+05	Ar-Ar
222.00	7.90e+05	Brunhes-Matuyama
241.63	9.15e+05	Ar-Ar
247.00	9.32e+05	Santa Rosa
271.50	9.87e+05	Upper Jaramillo
290.00	1.07e+06	Lower Jaramillo
313.00	1.12e+06	Panaruu
342.00	1.19e+06	Cobb Mt. top
347.00	1.22e+06	Cobb Mt. bottom

Refer to Lyons *et al.*[14] for more detail. Ages are in calendar years before present.